

PAPER

Waveguide Slot Array with Code-Division Multiplexing Function for Single RF Chain Digital Beamforming

Narihiro NAKAMOTO^{†a)}, *Member*, Kazunari KIHIRA[†], Toru FUKASAWA[†], *Senior Members*,
Yoshio INASAWA[†], *Member*, and Naoki SHINOHARA^{††}, *Senior Member*

SUMMARY This study presents a novel waveguide slot array with a code-division multiplexing function for single RF chain digital beamforming. The proposed antenna is comprised of a rectangular metallic waveguide's bottom part and a multilayer printed circuit board (PCB) with the rectangular waveguide's top wall and slot apertures. Multiple pairs of two symmetric longitudinal slots are etched on the metal surface of the PCB, and a PIN diode is mounted across each slot. The received signals of each slot pair are multiplexed in a code-division multiplexing fashion by switching the diodes' bias according to the Walsh Hadamard code, and the original signals are then recovered through a despreading process in the digital domain for digital beamforming. A prototype antenna with eight slot pairs has been fabricated and tested for proof of concept. The measured results show the feasibility of the proposed antenna.

key words: digital beamforming, waveguide slot array, single RF chain

1. Introduction

Digital beamforming (DBF) array antennas have been actively developed in recent years to meet the demands of modern wireless communication and radar systems [1]–[3]. In the conventional element-level DBF array antenna, each antenna element is connected to a separate radio frequency (RF) chain (amplifier, down-converter, and filter) and analog-to-digital converter (ADC) to obtain an individual complex received signal from each antenna element. Therefore, high hardware costs and increased power consumption make it difficult to realize a large-scale element-level DBF array antenna.

Many works have been reported to realize an element-level DBF array antenna that reduces the number of RF chains and ADCs [4]–[16]. To share a single RF chain among multiple antennas, received signals from multiple antennas are multiplexed into a single RF chain and ADC. Subsequently, each signal is recovered in the digital domain. In analogy with multiple access methods in wireless communication systems, three major multiplexing techniques, such as time-division multiplexing (TDM), frequency-division multiplexing (FDM), and code-division multiplexing (CDM), have been applied to realize a DBF array antenna with a single RF chain. In [4]–[7], received signals from each antenna

element are transferred to a single RF chain sequentially using switches in a TDM fashion. In [8] and [9], received signals from each antenna element are converted to signals with a different intermediate frequency (IF) from each other and then multiplexed in an FDM fashion. However, TDM and FDM schemes have a major drawback: when an adjacent channel interferer (ACI) is present, recovered signals in TDM and FDM schemes suffer from corruption by the ACI [10], [11].

CDM is the most promising method because, unlike TDM and FDM, the original signals can be recovered even in the presence of ACI [11]. In the CDM scheme, received signals from each antenna element are multiplied by spreading codes, and the spread signals are transferred to a single ADC. The original signals are recovered by a despreading process in the digital domain. In [11], received signals are code-modulated in the RF domain with a code-modulating low noise amplifier (LNA). In [12] and [13], code-modulation is performed in the IF domain with multipliers after amplification and frequency conversion of received signals. In these systems, each antenna element still requires a separate amplifier, which increases cost and power consumption in a large-scale array.

In [14], received signals are code-modulated with reflection-type $0^\circ/180^\circ$ phase shifters, and then all spread signals are combined by a microstrip power combiner and fed into a single RF chain. In [15], [16], a metasurface with a CDM function is presented. The responses of each unit cell are code-modulated by switching their integrated diodes, and then spread signals are spatially combined and fed into a feeding antenna with a single RF chain. In these antennas, signal amplification is implemented after combining the spread signals, and thus they can reduce the number of amplifiers.

In this study, we present a novel waveguide slot array antenna with a CDM function. The proposed antenna uses slot pairs with RF switches (e.g., PIN diodes) on the broad wall of a rectangular waveguide. Waveguide slot arrays with slots having integrated PIN diodes are presented in several studies [7], [17]–[19]. In [17]–[19], slots with appropriate radiation phases are activated, and the others are inactivated by switching the diodes' bias to achieve desired radiation patterns in the RF domain. In [7], only one slot is activated at a time, and an activated slot is sequentially switched by switching the diodes' bias. The original signal of each slot is then recovered in the digital domain in a TDM fashion.

Manuscript received July 27, 2023.

Manuscript revised October 19, 2023.

Manuscript publicized February 16, 2024.

[†]Mitsubishi Electric Corporatin, Kamakura-shi, 247-8501 Japan.

^{††}Research Institute for Sustainable Humansphere, Kyoto University, Uji-shi, 611-0011 Japan.

a) E-mail: Nakamoto.Narihiro@ap.MitsubishiElectric.co.jp

DOI: 10.23919/transcom.2023EBP3123

However, in the proposed antenna, the received signal of each slot-pair can be code-modulated by switching the RF switches' bias. Subsequently, the spread signals are combined in the hollow rectangular waveguide, and fed into a single RF chain. Following digitization, the despreading process recovers the original complex signals received by each slot pair, and the DBF is performed to achieve scanned beams, multiple beams, adaptive beams, or direction of arrival (DOA) estimation. To the best of our knowledge, this is the first waveguide slot array with a CDM function. The proposed antenna reduces the number of RF chains, amplifiers, and ADCs and has the potential to offer higher efficiency than previous works using microstrip lines or transmitarray/reflectorarray architecture [14], [15].

The rest of this paper is organized as follows: Section 2 explains the detailed configuration and operating principle of the proposed antenna; Sect. 3 describes the antenna design; Sect. 4 presents the experimental results of the prototype antenna; and Sect. 5 presents the conclusion.

2. Antenna Configuration and Operating Principle

Figure 1 shows the configuration of the proposed antenna with four slot pairs. The antenna comprises the bottom part of a metallic waveguide, a multilayer printed circuit board (PCB), RF switches, a single RF chain, an ADC, and a digital signal processing (DSP) unit. Both surfaces of the PCB are covered with copper foil, and slot apertures are formed by etching. Moreover, the back surface of the PCB is the top wall of the rectangular waveguide. A rectangular waveguide is formed by covering the bottom part of the metallic waveguide with the PCB. The waveguide is connected to the single RF chain through its feeding port. A slot pair comprises two longitudinal slots, which are offset symmetrically about the centerline of the waveguide, with the same dimensions. An RF switch is mounted across each slot aperture on the top surface of the PCB, and a DC bias line is printed on the inner layer of the PCB. The detailed configuration of the slot pair will be presented in Sect. 3.

The waveguide is here assumed to operate in only a single dominant mode (TE_{10} mode). In that case, the transverse currents along the top inner waveguide wall are symmetrical about the centerline of the waveguide [20]. Because the longitudinal slot radiates by interrupting the transverse current, the field radiated by each slot of the slot pair has the same amplitude in anti-phase to each other. In the proposed antenna, one RF switch of each slot pair is turned off (OFF state), and the other is turned on (ON state), allowing one slot to receive an incident wave, whereas the other cannot. Therefore, the phase of the received signal of each slot pair can be reversed by switching the RF switches' state. The states of each switch are sequentially controlled according to high-speed spreading codes, and the received signal of each slot pair is code-modulated and spectrum-spread. Subsequently, spread signals are combined in the rectangular waveguide and fed into a single RF chain and an ADC. Following digitization, the original complex signals received by

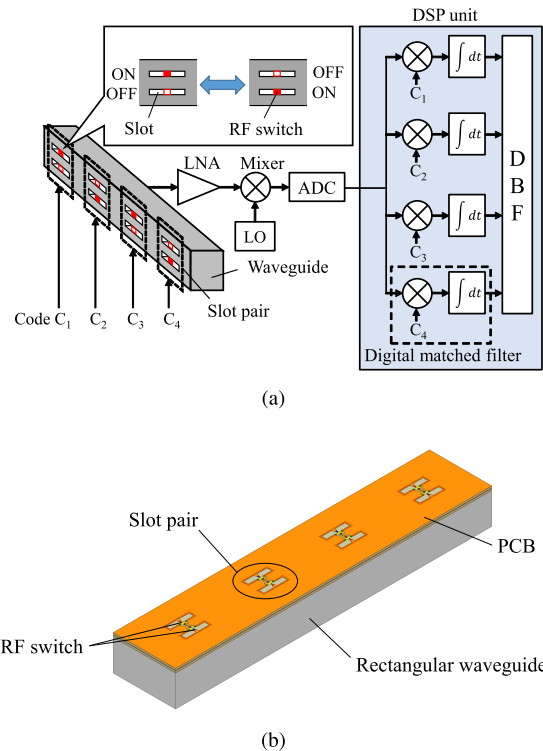


Fig. 1 Configuration of the proposed antenna. (a) Block diagram and (b) perspective view of the waveguide slot array.

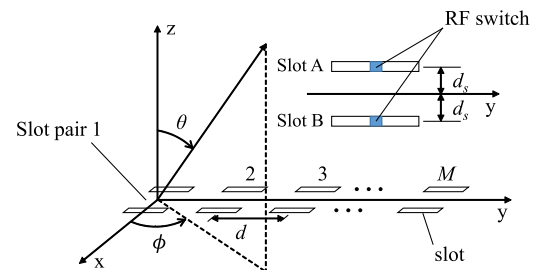


Fig. 2 Radiating aperture of the proposed antenna with M slot pairs.

each slot pair are demultiplexed by the despreading process in the DSP unit and then used for further beamforming or DOA estimation with DSP.

To understand the operating principle and signal-to-noise ratio (SNR) performance of the proposed antenna, we now present a mathematical model of the proposed antenna. Figure 2 illustrates a coordinate system of the radiating aperture of the proposed antenna. M slot pairs are arranged parallel to the y -axis, and each slot is offset by $\pm d_s$ from it. Each slot is now assumed to have a radiation pattern given by

$$f^{(\pm)}(\theta, \phi) = f_m(\theta, \phi) e^{\pm j k_0 d_s \sin \theta \cos \phi} \quad (1)$$

where the superscripts (+) and (−) indicate the radiation pattern of the slot A and B, respectively, $f_m(\theta, \phi)$ is the far-field vector of the m th slots, and k_0 is the free space wavenumber. We consider that a plane wave arrives at the antenna with an incident angle of θ in the $y-z$ plane ($\phi =$

$\pi/2$). In this case, the received signal of the m th slot pair is given by

$$r_m(t) = c_m(t)f_{m\phi}s_m(t)e^{j2\pi f_c t} \quad (2)$$

where $f_{m\phi}$ is the ϕ -component of $f_m(\theta, \phi)$ in the y - z plane (we ignore the cross-polarization component), f_c is the carrier frequency, $s_m(t)$ is an incident signal to the slot pair, and $c_m(t)$ is a designated spreading code and indicates an operating state of the slot pair: $c_m(t) = 1$ when the slot A is activated and $c_m(t) = -1$ when the slot B is activated. Here we assume that the slot with an RF switch in the ON state is perfectly inactivated and does not receive any signals.

All the received signals $r_m(t)$ (for $1 \leq m \leq M$) are combined by the waveguide, and the output signal is then amplified by an LNA. The resultant signal is expressed as

$$R(t) = g \left[\sum_{m=1}^M \alpha_m r_m(t) + n(t) \right] \quad (3)$$

where α_m is the transmission characteristics of each slot pair through the waveguide, g is the gain of the LNA, and $n(t)$ is the white Gaussian noise referred to the input of the LNA. $R(t)$ is then downconverted to the baseband, and the baseband signal is given by

$$R_b(t) = g \left[\sum_{m=1}^M \alpha_m f_{m\phi} c_m(t) s_m(t) + n(t) \right]. \quad (4)$$

Following digitization, the signal is separated into I and Q components by a digital IQ demodulator, but we ignore the IQ demodulator and show only a single path for simplicity in Fig. 1(a). The signal is then input to M digital matched filters for the despreading process, where the m th matched filter is matched to the m th spreading code. When we assume that the incident signal $s_m(t)$ varies more slowly than the spreading code $c_m(t)$, the output signal $S_m(t)$ of the m th matched filter is expressed as

$$S_m(t) = \frac{1}{T_b} \int_0^{T_b} R_b(t) c_m(t) dt = S_{m,d}(t) + S_{m,i}(t) \quad (5)$$

$$S_{m,d}(t) = g \alpha_m f_{m\phi} C_{m,m} s_m(t) \quad (6)$$

$$S_{m,i}(t) = g \sum_{m' \neq m} \alpha_{m'} f_{m'\phi} C_{m,m'} s_{m'}(t) + \frac{g}{T_b} \int_0^{T_b} n(t) c_m(t) dt \quad (7)$$

where T_b is the symbol duration, and \sum' indicates a summation from $m' = 1$ to M except for $m' = m$. $S_{m,d}(t)$ represents the desired signal for the m th slot-pair, whereas $S_{m,i}(t)$ is the interference from other signals and noise. $C_{m,m'}$ is the cross-correlation of the spreading codes and is defined as

$$C_{m,m'} = \frac{1}{T_b} \int_0^{T_b} c_m(t) c_{m'}(t) dt. \quad (8)$$

In (7), the first term of the right side is the interference from other signals, and a spreading code with $C_{m,m'} = 0$ must be used to minimize $S_{m,i}(t)$. Therefore, although there are

several options for the spreading codes [21], the perfectly orthogonal codes, namely the Walsh-Hadamard (WH) codes (see Appendix A), with a length of $L_c \geq M$ must be used as the spreading codes. When we assume that synchronization between spreading and despreading is achieved, the orthogonality is satisfied for the WH codes as follows:

$$C_{m,m'} = \begin{cases} 1 & \text{for } m = m' \\ 0 & \text{for } m \neq m', \end{cases} \quad (9)$$

and $S_{m,d}(t)$ and $S_{m,i}(t)$ are reduced to

$$S_{m,d}(t) = g \alpha_m f_{m\phi} s_m(t) \quad (10)$$

$$S_{m,i}(t) = \frac{g}{T_b} \int_0^{T_b} n(t) c_m(t) dt. \quad (11)$$

As expected, the original signal can be perfectly recovered for the WH codes. The SNR at each element output becomes

$$SNR_m = \frac{|\alpha_m|^2 G_m P_s}{\sigma_n^2} \quad (12)$$

where $P_s = E[|s_m(t)|^2]$, $\sigma_n^2 = E[|n(t)|^2]$ ($E[\cdot]$ is an expectation operator), and $G_m = |f_{m\phi}|^2$ is the gain of each slot pair (see Appendix B). Similarly, SNR at the array output is given as

$$SNR_a = \frac{M \alpha_0^2 G_e P_s}{\sigma_n^2} \quad (13)$$

where we assume that $|\alpha_m| = \alpha_0$ and $G_m = G_e$ for all slot pairs. For the hollow waveguide, $|\alpha_m|^2 = \alpha_0^2 \simeq 1/M$ in (12) and (13), and thus the SNRs are degraded to $1/M$ of those for the element-level DBF array antenna or the previous works in [11] and [12]. This is because the signal amplification is performed after signal combination, and the signal power of each slot pair is degraded due to the insertion loss of the waveguide combiner. This SNR degradation is a drawback of the proposed antenna, and there is another restriction. When we use the spreading code with length L_c , the chip duration becomes T_b/L_c . Therefore, the ADC sampling rate and PIN diode's switching rate must be faster than M/T_b . Thus, the available ADC sampling rate and PIN diode's switching speed dictate the maximum number of multiplexing signals and maximum symbol rate in the proposed antenna.

Although we have here considered the receiving antenna, the same idea is applicable to a transmitting antenna. In that case, the transmitting signals from each slot-pair are code-modulated in the digital domain and recovered by the despreading process by switching the RF switches' bias. However, there are some difficult problems for the transmitting antenna such as spurious emissions and power handling capability of the RF switch, which will hinder practical application. Therefore, we focus only on the receiving antenna in this study. In addition, we here assume that the incident wave lies in the y - z plane. For other incident angles out of this plane, the factor $e^{\pm j k_0 d_s \sin \theta \cos \phi}$ remains in (2), which introduces errors in the spreading process. The effect of these errors will be discussed in Sect. 4.

3. Antenna Design

We designed a prototype waveguide slot array with eight slot pairs as a proof of concept of the proposed antenna. Figure 3 demonstrates a detailed configuration of a slot pair for the prototype antenna. Each slot pair and its DC bias line are printed on a 4-layers PCB. The conductor layers are denoted as L1–L4, and two substrates with a thickness of 0.75 mm are bound with a prepreg. The total thickness of the PCB is 1.67 mm. Megtron6 ($\epsilon_r = 3.6$ and $\tan \delta = 0.003$) by Panasonic Industry is selected as a substrate material. Slot apertures with a length of L_s and a width of w_s are formed by etching all the layers. Additionally, multiple through-hole vias with a diameter of 0.4 mm are placed around the slot

apertures at 0.7 mm intervals to prevent RF leakage into the parallel plate mode between layers.

PIN diode (SMP1345-079LF by Skyworks) is used as an RF switch. A single PIN diode is placed across each slot at its center on the L1 layer. DC bias lines of each PIN diode are printed on the L2 layer and connected to the bias circuit (not shown in Fig. 3). An RF choke inductor of 15 nH (LQW15AN15NG00 by Murata Manufacturing) is placed between the PIN diode and the bias line to prevent the RF leakage into the bias line. Two DC block capacitors of 1.2 pF (GJM1555C1H1R2WB01 by Murata Manufacturing) are placed between the component pad and the ground to isolate the bias line from the ground. In the proposed antenna, one diode of each slot pair is reverse biased (OFF state), and the other is forward biased (ON state). When the PIN diode is in the OFF state, it approximates an open circuit and has minimal effect on the radiation characteristics of the slot. In contrast, when the PIN diode is in the ON state, it approximately short-circuits the slot at its center, effectively deactivating it.

The inter-element spacing d , distance between the centers of adjacent slot pairs, is set to 33.1 mm for the prototype antenna to have a field of view of $\pm 15^\circ$ without any grating lobes at the operating frequency of 7 GHz. A standing-wave waveguide slot array is adopted in the prototype antenna, and the dimensions of the bottom part of metallic waveguide is designed such that a guided wavelength becomes twice the inter-element spacing. We select a single-ridged waveguide, and the designed dimensions are listed in Table 1.

A slot pair with the integrated components is designed using the electromagnetic simulator Ansys HFSS. In the prototype antenna, we use slot pairs with identical dimensions to simplify the antenna design, and we determine them such that the slots resonate at 7 GHz with an appropriate radiation conductance for impedance matching. The aperture distribution would degrade due to this simplified design. However, we accept it here because the signal variations among the slot pairs caused by it can be calibrated in the digital domain after demultiplexing. In the simulations, the PIN diode is modeled as an equivalent circuit of lumped elements to consider its effect on the slot performance. Specifically, the PIN diode in the ON state is modeled as a series circuit of a 2.0 Ω resistor and a 0.7 nH inductor, whereas one in the OFF state is modeled as a 0.13 pF capacitor [22], [23]. The designed dimensions of a slot pair are shown in Table 1.

Figure 4 depicts an exploded view of the prototype

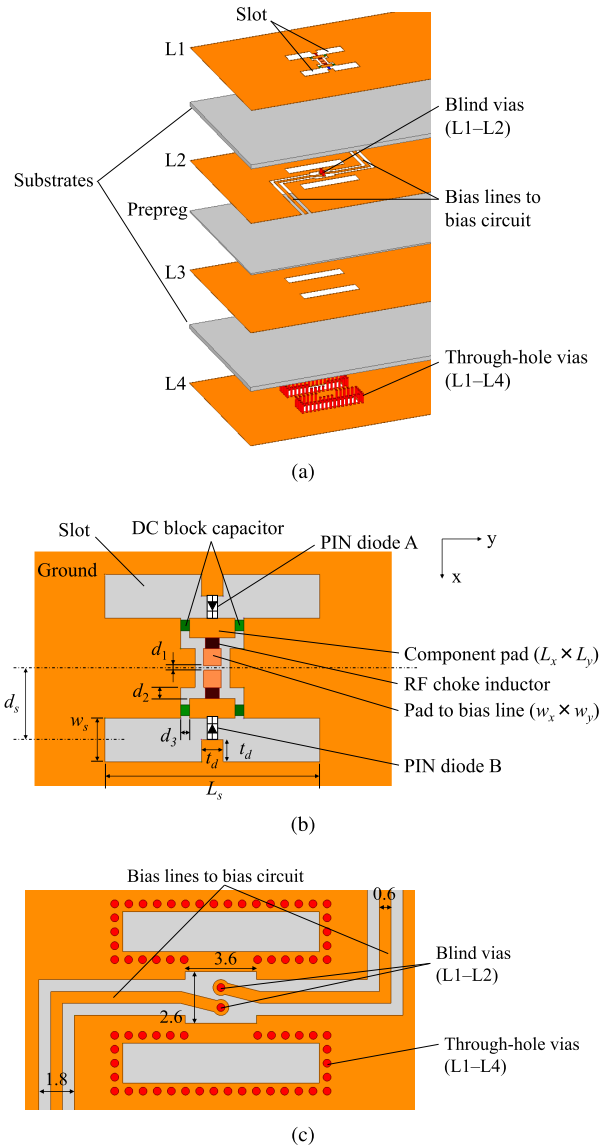


Fig. 3 Configuration of a slot pair for the prototype antenna. (a) Expanded view of the PCB, (b) detailed configuration of slot pair with PIN diodes, RF choke inductors, and DC block capacitors, and (c) layout of the L2 layer.

Table 1 Dimensions of the prototype antenna.

| Parameter | Value [mm] | Parameter | Value [mm] |
|--------------|------------|-------------------|------------|
| Waveguide | | Pad and clearance | |
| inner width | 23.0 | L_x | 0.9 |
| inner height | 11.5 | L_y | 2.1 |
| ridge height | 5.0 | w_x | 0.8 |
| ridge width | 1.0 | w_y | 0.8 |
| Slot-pair | | d_1 | 0.2 |
| L_s | 9.9 | d_2 | 0.5 |
| w_s | 2.0 | d_3 | 0.4 |
| d_s | 3.3 | t_d | 1.0 |

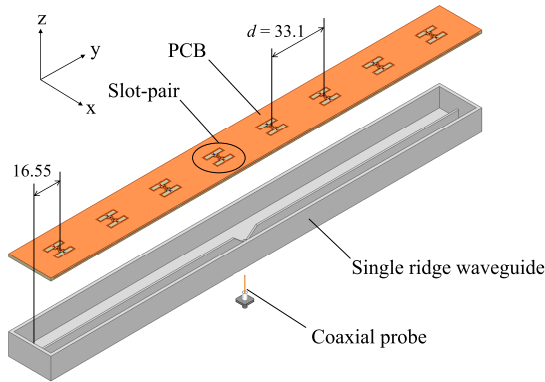


Fig. 4 Exploded view of the prototype waveguide slot array (dimensions in millimeter).

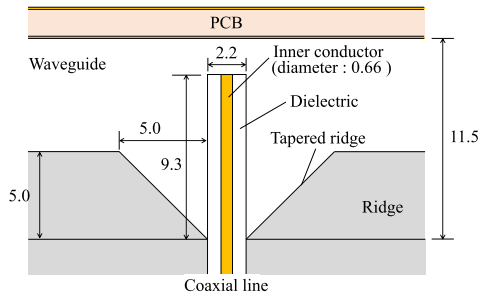


Fig. 5 Configuration of the designed transition from the coaxial line to the single-ridged waveguide (dimensions in millimeter).

antenna. Eight designed slot pairs are arranged linearly, and both ends of the ridge waveguide are short-circuited at 16.55 mm away from the center of the end slot pairs. The ridge waveguide is fed by an SMA coaxial probe inserted at its center from its bottom side. Figure 5 shows the detailed structure of the transition from the coaxial line to the ridge waveguide. The coaxial inner conductor and the dielectric are extended into the waveguide, and the ridges are linearly tapered at the transition to achieve impedance matching.

4. Experiments

The prototype antenna was fabricated and tested to verify the feasibility of the proposed antenna. Figure 6 shows photos of the fabricated antenna. The prototype antenna was installed in a ground plane of dimension 400 mm×400 mm. Bias lines for PIN diodes were connected to bias circuits (DC power suppliers) through biasing wires. The PIN diodes were forward biased with the forward current of 10 mA and were reverse biased with the reverse voltage of 22 V.

Here we consider that a continuous wave (CW) with an amplitude s_0 impinges on the proposed antenna with the incident angle θ in the y - z plane. The incident signal to the m th slot pair is given by $s_m(t) = s_0 e^{jk_0 m d \sin \theta}$, and thus the recovered desired signal (10) becomes $S_{m,d}(t) = g \alpha_m s_0 f_{m\phi} e^{jk_0 m d \sin \theta}$ and is proportional to the element pattern of the m th slot pair. In the experiment, therefore, CWs at 7 GHz were transmitted and received while changing θ ,

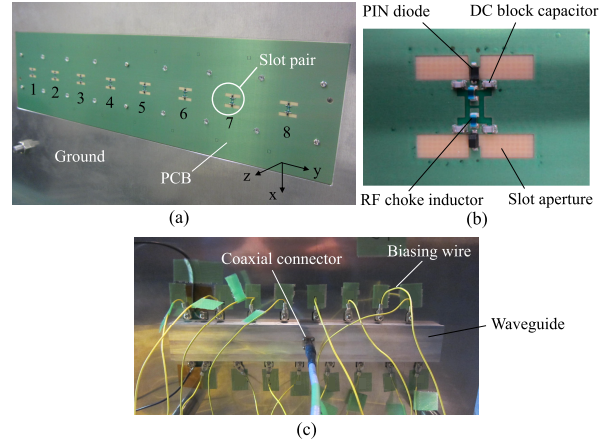


Fig. 6 Fabricated prototype antenna.

and we then compared the recovered signals by the prototype antenna with simulated element patterns. The measurement was performed using a compact antenna test range setup in an anechoic chamber. CW transmission and reception, transmission coefficient (S_{21}) measurement, between a transmitting antenna and the prototype one was conducted with a vector network analyzer. To change the incident angle θ , the prototype antenna was rotated around the x -axis, which passed through the waveguide center, with a rotary positioner. For a proof of concept, we manually switched the biasing state of each PIN diode to the specified states described later and measured the S_{21} at various θ (from -90° to 90° in 0.1° increments) in each state. Subsequently, we recovered the received signal e_m of each slot-pair from the measured signals at θ by the following expression:

$$e_m(\theta) = \frac{1}{L_c} \sum_{l=1}^{L_c} E_l(\theta) c_m(l) \quad (14)$$

where $E_l(\theta)$ and $c_m(l)$ are the measured S_{21} at θ and the designated spreading code for the m th slot pair at the l th state, respectively. This process was performed in software. We assumed that synchronization between spreading and despreading was perfectly achieved and ignored the transient characteristics of the PIN diodes. We used the WH codes with $L_c = 8$ or 16 as the spreading codes in the experiment. Figure 7 demonstrates the relationship between the WH codes with $L_c = 8$ and the positions of activated slots (with the PIN diode in the OFF state). In the 1st state, the activated slots were located to be excited in phase at 7 GHz. We assigned this arrangement to +1 of each code and determined the positions of activated slots for the other states. For the WH codes with $L_c = 16$, we avoided using the WH code whose elements were all +1 for a reason discussed later and used the codes corresponding to the 2nd to 10th rows of the Hadamard matrix (see Fig. A.1). We determined the positions of the activated slots for the WH codes with $L_c = 16$ in a similar manner to $L_c = 8$, and we here omit the detailed arrangement.

| Slot-pair number | WH code | State number | | | | | | | |
|------------------|----------------------------------|--------------|---|---|---|---|---|---|---|
| | | 1 | 2 | 3 | 4 | 5 | 6 | 7 | 8 |
| 1 | $c_1 = (+, +, +, +, +, +, +, +)$ | ■ | ■ | ■ | ■ | ■ | ■ | ■ | ■ |
| 2 | $c_2 = (+, -, +, -, +, -, +, -)$ | ■ | □ | ■ | □ | ■ | □ | ■ | □ |
| 3 | $c_3 = (+, +, -, -, +, +, -, -)$ | ■ | ■ | □ | □ | ■ | ■ | □ | □ |
| 4 | $c_4 = (+, -, -, +, +, -, -, +)$ | ■ | □ | □ | ■ | ■ | □ | □ | ■ |
| 5 | $c_5 = (+, +, +, +, -, -, -, -)$ | ■ | ■ | ■ | ■ | □ | □ | □ | □ |
| 6 | $c_6 = (+, -, +, -, -, +, -, +)$ | ■ | □ | ■ | □ | □ | ■ | □ | ■ |
| 7 | $c_7 = (+, +, -, -, -, +, -, +)$ | ■ | ■ | □ | □ | □ | ■ | ■ | □ |
| 8 | $c_8 = (+, -, -, +, -, +, -, -)$ | ■ | □ | □ | ■ | □ | □ | ■ | □ |

Fig. 7 Positional relationship between the WH codes with $L_c = 8$ and the activated slots (+ and - indicate +1 and -1, respectively).

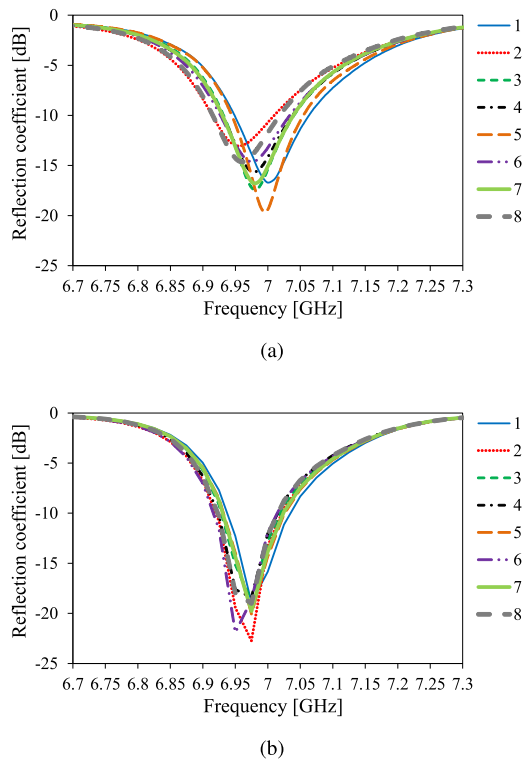


Fig. 8 Reflection coefficients in each state for the WH codes with $L_c = 8$: (a) Measurement and (b) simulation.

4.1 Experimental Results

Figures 8(a) and (b) show the measured and simulated reflection coefficients at each state for the WH codes with $L_c = 8$, respectively. Although there are some discrepancies between the measured and simulated reflection coefficients, the prototype antenna has a reflection coefficient of less than -10 dB at the operating frequency in all states. The causes for the discrepancies seem to be fabrication errors and errors in electrical properties of the integrated components. The

reflection coefficients vary depending on the states due to the variation of the active admittance of each slot pair. The prototype antenna has a bandwidth of only 1.5% with a reflection coefficient of less than -10 dB, and thus a bandwidth enhancement is one of the future works. The bandwidth of the slot can be improved by replacing the PCB material with one with a low dielectric constant, and the slot array's bandwidth can be improved by replacing its series-feed structure with a corporate-feed type [24]. Since the measured reflection coefficients for the WH codes with $L_c = 16$ were almost the same as those with $L_c = 8$, we here omit the detailed results. The measured gain in the broadside direction at 7 GHz for the 1st state, corresponding to an ordinary probe-fed waveguide slot array, is 11.1 dBi, and the estimated radiation efficiency is approximately 47%. The loss due to the reverse parallel resistance R_p of the PIN diode is a significant factor in the reduction in radiation efficiency. R_p of the PIN diode for the prototype antenna is estimated to be approximately 10 k Ω by simulations. We can improve the radiation efficiency by replacing the PIN diode with one with a larger R_p , which is also a future challenge.

Figure 9(a) shows the recovered signals of the 1st to 4th slot pairs at each sample angle from the measured S_{21} at 7 GHz for the WH codes with $L_c = 8$. In addition, recovered signals from the simulated S_{21} and simulated individual element patterns of each slot pair are shown in Fig. 9(a). Due to the symmetry of the antenna structure, the recovered signals of the 5th to 8th slot pairs have similar patterns, which we omit here due to space constraints. The amplitudes of each signal are normalized by their respective peak amplitudes, and the phases are calibrated to be 0 deg. in the broadside direction. The recovered signals of each slot pair agree well with their respective element pattern in simulation, whereas there are some discrepancies in measurement. Particularly, there are larger discrepancies between measured and simulated recovered signals for the 1st slot pair, and we find that demultiplexing is not working well. We will later discuss the cause of this deterioration in recovered signals. Similarly, Fig. 9(b) shows the recovered signals with the WH codes with $L_c = 16$. In this case, the recovered signals from the measured S_{21} agree with simulated element patterns for all slot pairs. Although there are some discrepancies between measured and simulated recovered signals, the prototype antenna is successful in demultiplexing.

4.2 Discussions

We first discuss the effect of the differences in properties of each PIN diode on the recovered signals to reveal the cause of the deterioration in the recovered signals of the 1st slot-pair with the WH codes with $L_c = 8$.

We now consider the same model as that in Sect. 2. When the PIN diodes have errors in their electrical properties, the received signal of each slot-pair deviates from its ideal. Now consider δ be the fractional error of the received signal due to the errors in the PIN diode's properties, and the received signal $r'_m(t)$ of the m th slot pair under these errors

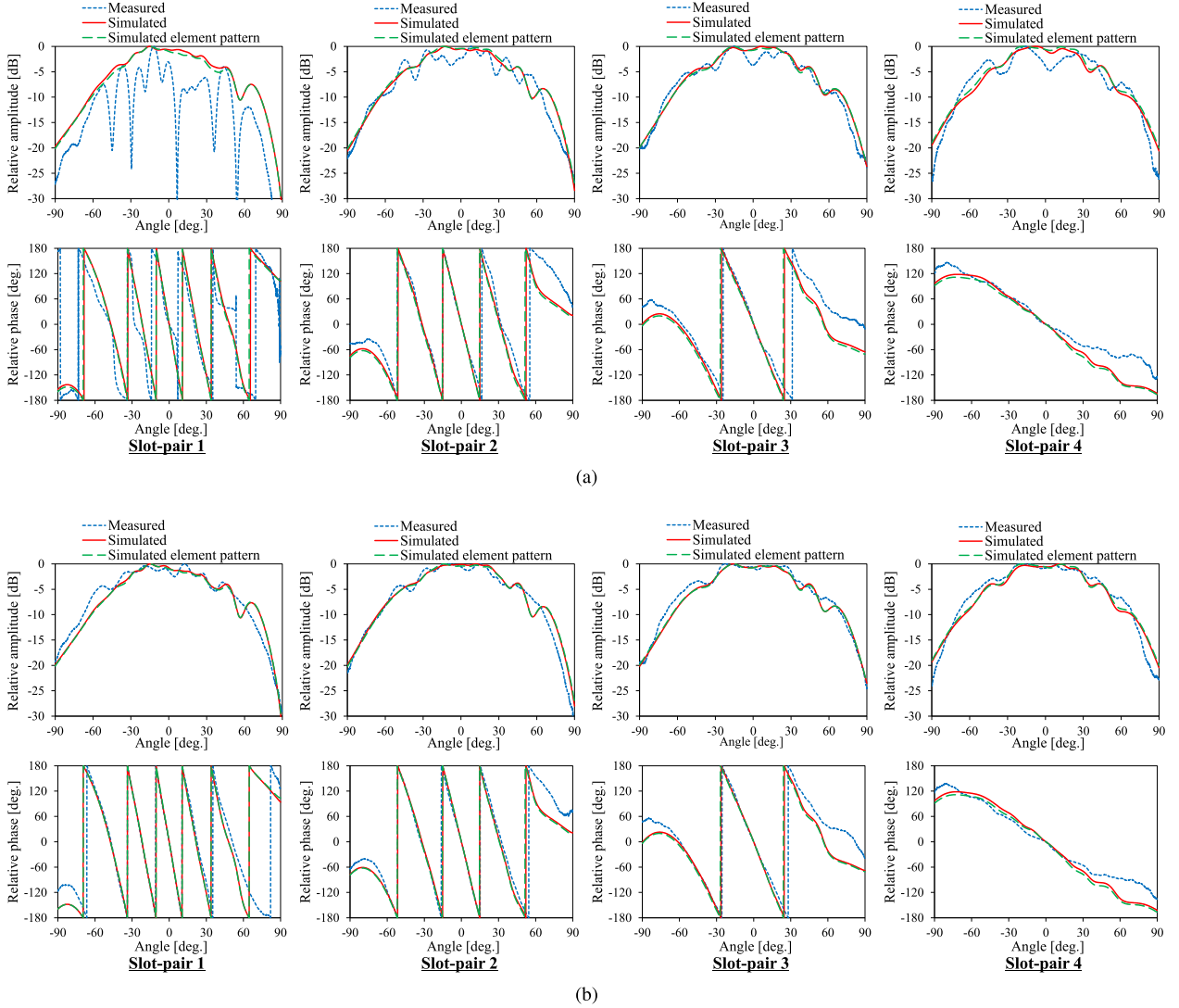


Fig. 9 Recovered signals of the 1st to 4th slot-pairs with the WH codes with (a) $L_c = 8$ and (b) $L_c = 16$ at 7 GHz. Blue dashed and red solid lines indicate the recovered signals from the measured and simulated S_{21} , respectively, and long-dashed green lines indicate the simulated element patterns of each slot pair. The amplitude and phase patterns are shown in the upper and lower rows, respectively.

is then expressed by

$$r'_m(t) = \{1 + \delta_m(t)\} r_m(t). \quad (15)$$

The errors depend on the operating states of the slot pair, and we denote that $\delta_m(t) = \delta_m^{(\pm)}$ when the slot corresponding to ± 1 is activated. Replacing $r_m(t)$ in (3) with $r'_m(t)$ and using (4) and (5), we obtain the following recovered signals:

$$S'_{m,d}(t) = \frac{g\alpha_m f_m \phi s_m(t)}{T_b} \times \int_0^{T_b} c_m^2(t) \{1 + \delta_m(t)\} dt \quad (16)$$

$$S'_{m,i}(t) = \frac{g}{T_b} \sum' \alpha_{m'} f_{m'} \phi s_{m'}(t) \times \int_0^{T_b} c_{m'}(t) \{1 + \delta_{m'}(t)\} c_m(t) dt \quad (17)$$

where we ignore the noise for simplicity. When we consider a case where the WH code whose elements are all +1 is used for the m th slot-pair, (16) and (17) are reduced to

$$S'_{m,d}(t) = g\alpha_m f_m \phi s_m(t) (1 + \delta_m^{(+)}) \quad (18)$$

$$S'_{m,i}(t) = \frac{g}{2} \sum' \alpha_{m'} f_{m'} \phi s_{m'}(t) (\delta_{m'}^{(+)} - \delta_{m'}^{(-)}). \quad (19)$$

According to (19), $S'_{m,i}(t) \neq 0$ when $\delta_m^{(+)} \neq \delta_{m'}^{(-)}$, and thus the recovered signal suffers from the remaining interference from other slot-pairs' signals. However, when the WH codes, including both +1 and -1, are used for the m th slot pair, (16) and (17) are given by

$$S'_{m,d}(t) = g\alpha_m f_m \phi s_m(t) \left(1 + \frac{\delta_m^{(+)} + \delta_m^{(-)}}{2}\right) \quad (20)$$

$$S'_{m,i}(t) = 0. \quad (21)$$

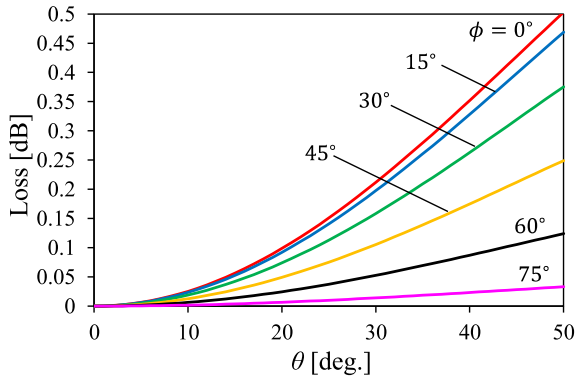


Fig. 10 Calculated losses due to the factor $\cos(k_0 d_s \sin \theta \cos \phi)$.

Because $c_m(t)$ and $c_{m'}(t)\{1 + \delta_m(t)\}$ are also orthogonal when $m \neq 1$ (see Appendix A), the interference from other slot-pairs' signals disappear in (21). Therefore, in an actual situation where the PIN diodes have errors in their electrical properties, we must use the WH codes including both +1 and -1, with a length of $L_c > M$, to prevent deterioration in recovered signals.

Next, we consider that a plane wave arrives at the antenna with an incident angle (θ, ϕ) out of the y - z plane in Fig. 2. In this case, the received signal $r_m''(t)$ is given by

$$r_m''(t) = c_m(t) f_m e^{\pm j k_0 d_s \sin \theta \cos \phi} s_m(t) e^{j 2 \pi f_c t} \quad (22)$$

where $f_m = |f_m(\theta, \phi)|$, and we assume that the polarization of the antenna is matched to that of the incident plane wave. In (22), the factor $e^{\pm j k_0 d_s \sin \theta \cos \phi}$ causes an error depending on the operating state of the slot pair for the received signals. The effect of this error can be evaluated with (20) by replacing $\delta_m^{(\pm)}$ and $f_{m\phi}$ by $(e^{\pm j k_0 d_s \sin \theta \cos \phi} - 1)$ and f_m , respectively, and the recovered signal becomes

$$S_{m,d}''(t) = g \alpha_m f_m s_m(t) \cos(k_0 d_s \sin \theta \cos \phi). \quad (23)$$

The factor $\cos(k_0 d_s \sin \theta \cos \phi)$ introduces an additional loss into the recovered signal depending on the incident angle. Figure 10 shows calculated losses with various incident angles for the prototype antenna. The prototype antenna suffers from larger losses when ϕ is around 0° (for example, the loss of 0.43 dB for $(\theta, \phi) = (45^\circ, 0^\circ)$). Slot pairs with a smaller slot offset should be used to mitigate this loss, and it requires miniaturizing slot pairs. Slot offset is closely related to slot admittance and mounting space for the inductors and capacitors. Therefore, miniaturization of the slot pair is also one of the future challenges.

4.3 Application Example: DOA Estimation

Simulation tests of DOA estimation are performed to demonstrate the feasibility of DBF function by the prototype antenna. In the simulation, the one-dimensional MUSIC algorithm [25] is employed, and the received signal of the antenna is calculated using the measured S_{21} . Thus, received signals at the l th state of the prototype antenna are calculated by

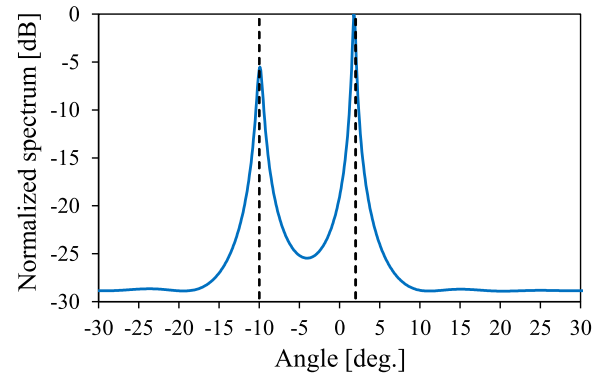


Fig. 11 Simulated MUSIC spatial spectrum for two uncorrelated incident signals with $(\theta_1, \theta_2) = (-10.0^\circ, 2.0^\circ)$ and SNR = 20 dB.

$$R_b(t) = \sum_{k=1}^K s^{(k)}(t, \theta_k) E_l(\theta_k) + n(t) \quad (24)$$

where $s^{(k)}(t, \theta_k)$ represents the k th incident signal to the antenna, θ_k is its incident angle, and K is the number of the incident signals. Recovered signals $S_m(t)$ are calculated by (5), and the MUSIC spectrum is then calculated by [25]

$$P_{MU}(\theta) = \frac{1}{\mathbf{a}^H(\theta) \mathbf{E}_n \mathbf{E}_n^H \mathbf{a}(\theta)} \quad (25)$$

where the superscript H represents the Hermitian transpose operation, $\mathbf{a}(\theta) = [C_1 e^{-j k_0 d \sin \theta}, \dots, C_M e^{-j k_0 M d \sin \theta}]$, and C_m are calibration weights and are determined using a reference signal from $\theta = 0^\circ$, ignoring the mutual coupling effect for simplicity. \mathbf{E}_n is a matrix whose columns are the noise eigenvectors of the covariance matrix $\mathbf{R} = E[\mathbf{S}(t) \mathbf{S}^H(t)]$ where $\mathbf{S}(t) = [S_1(t), \dots, S_M(t)]^T$, and the superscript T represents the transpose operation.

Here, we consider two uncorrelated QPSK modulated incident signals with the same power. The incident angles are $(\theta_1, \theta_2) = (-10.0^\circ, 2.0^\circ)$. The operating state of the antenna is switched 16 times during each symbol according to the WH codes with $L_c = 16$. We assume that synchronization between spreading and despreading is perfectly achieved. The covariance matrix \mathbf{R} is calculated using recovered signals of 100 symbols. Figure 11 shows the calculated MUSIC spatial spectrum for SNR = 20 dB. We can find two obvious peaks in the spectrum, and estimated incident angles are -10.0° and 1.8° , which agree well with the actual ones. The estimation error would be due to an effect of mutual couplings between slot pairs and imperfection in demultiplexing.

5. Conclusion

In this study, we presented a novel waveguide slot array with slot pairs for the CDM function. The received signals of each slot pair are multiplexed in the CDM fashion by switching the diodes' bias according to the WH codes, and they are recovered through the despreading process in the digital domain for further DSP. We also presented the

operating principle of the proposed antenna using the mathematical model, and then designed, fabricated, and tested a proof of concept prototype antenna with eight slot pairs. Although we manually switched the PIN diodes' bias, ignored the transient characteristics of the PIN diodes, and assumed perfect synchronization between spreading and despreading, the experimental results demonstrated the feasibility of the proposed antenna. We also showed that the WH codes including both +1 and -1, with a length of $L_c > M$, must be used to prevent recovered signals' deterioration due to errors in the PIN diodes' electrical properties.

Future works of the proposed antenna include further tests considering the transient characteristics of the PIN diodes and actual synchronization issues, bandwidth enhancement, radiation efficiency improvement, and miniaturization of the slot pair for mitigating the losses depending on the incident angle of signals. The proposed antenna has the potential to provide a single RF Chain DBF antenna with lower cost and higher radiation efficiency.

References

- [1] C. Fulton, M. Yearly, D. Thompson, J. Lake, and A. Mitchell, "Digital phased arrays: Challenges and opportunities," *Proc. IEEE*, vol.104, no.3, pp.487–503, March 2016.
- [2] P.K. Bailleul, "A new era in elemental digital beamforming for spaceborne communications phased arrays," *Proc. IEEE*, vol.104, no.3, pp.623–632, March 2016.
- [3] B. Yang, Z. Yu, J. Lan, R. Zhang, J. Zhou, and W. Hong, "Digital beamforming-based massive MIMO transceiver for 5G millimeter-wave communications," *IEEE Trans. Microw. Theory Techn.*, vol.66, no.7, pp.3403–3418, July 2018.
- [4] J.D. Fredrick, Y. Wang, and T. Itoh, "Smart antennas based on spatial multiplexing of local elements (SMILE) for mutual coupling reduction," *IEEE Trans. Antennas Propag.*, vol.52, no.1, pp.106–114, Jan. 2004.
- [5] K. Koga, N. Kikuma, H. Hirayama, K. Sakakibara, T. Koike, H. Iwasaki, and Y. Mizuno, "A study of switching methods for an adaptive array with a single receiver using time-division multiplexing," *Trans. IEICE Commun. (Japanese Edition)*, vol.J96-B, no.2, pp.149–162, Feb. 2013.
- [6] S. Henault, B.R. Jackson, and Y.M.M. Antar, "Compensation of time-division multiplexing distortion in switched antenna arrays with a single RF front-end and digitizer," *IEEE Trans. Antennas Propag.*, vol.61, no.8, pp.4383–4388, Aug. 2013.
- [7] Y. Yashchyshyn, K. Derzakowski, P.R. Bajurko, J. Marczewski, and S. Kozłowski, "Time-modulated reconfigurable antenna based on integrated S-PIN diodes for mm-Wave communication systems," *IEEE Trans. Antennas Propag.*, vol.63, no.9, pp.4121–4131, Sept. 2015.
- [8] M.A. Johnson, "Phased-array beam steering by multiplex sampling," *Proc. IEEE*, vol.56, no.11, pp.1801–1811, Nov. 1968.
- [9] N. Akram, A. Madanayake, S. Pulipati, V. Ariyaratna, S.B. Venkatakrishnan, D. Psychogiou, J. Volakis, T.S. Rappaport, and T.L. Marzetta, "Frequency-multiplexed array digitization for MIMO receivers: 4-antennas/ADC at 28 GHz on Xilinx ZCU-1285 RF SoC," *IEEE Access*, vol.9, pp.142743–142753, 2021.
- [10] A. Jahanian, F. Tzeng, and P. Heydari, "Code-modulated path-sharing multi-antenna receivers: Theory and analysis," *IEEE Trans. Wireless Commun.*, vol.8, no.5, pp.2193–2201, May 2009.
- [11] F. Tzeng, A. Jahanian, D. Pi, and P. Heydari, "A CMOS code-modulated path-sharing multi-antenna receiver front-end," *IEEE J. Solid-State Circuits*, vol.44, no.5, pp.1321–1335, May 2009.
- [12] E.A. Alwan, A. Akhlayat, M. LaRue, W. Khalil, and J.L. Volakis, "Low cost, power efficient, on-site coding receiver (OSCR) for ultra-wideband digital beamforming," 2013 IEEE Int. Symp. Phased Array Systems Tech., pp.202–206, 2013.
- [13] S.B. Venkatakrishnan, D.K. Papantonis, A.A. Akhlayat, E.A. Alwan, and J.L. Volakis, "Experimental validation of on-site coding digital beamformer with ultra-wideband antenna arrays," *IEEE Trans. Microw. Theory Techn.*, vol.65, no.11, pp.4408–4417, Nov. 2017.
- [14] J. Zhang, W. Wu, and D.-G. Fang, "Single RF channel digital beamforming multibeam antenna array based on time sequence phase weighting," *IEEE Antennas Wireless Propag. Lett.*, vol.10, pp.514–516, 2011.
- [15] X. Wang and C. Caloz, "Direction-of-arrival (DOA) estimation based on spacetime-modulated metasurface," 2019 IEEE Int. Symp. Antennas Propag. and USNC-URSI Radio Science Meeting, pp.1613–1614, 2013.
- [16] X. Wang and C. Caloz, "Pseudorandom sequence (space-) time-modulated metasurfaces: Principles, operations, and applications," *IEEE Antennas Propag. Mag.*, vol.64, no.4, pp.135–144, Aug. 2022.
- [17] Y. Yashchyshyn, J. Marczewski, K. Derzakowski, J.W. Modelski, and P.B. Grabcic, "Development and investigation of an antenna system with reconfigurable aperture," *IEEE Trans. Antennas Propag.*, vol.57, no.1, pp.2–8, Jan. 2009.
- [18] Z. Zhou, H. Su, B. Yang, S. Wu, and X.Y. Zhang, "Digital encoding holographic antenna based on SIW waveguide," 2021 IEEE Int. Workshop on Electromagnetics: Applications and Student Innovation Competition (iWEM), 2021.
- [19] H. Li, S. Li, B. Hou, X. Zhang, W. Wen, and C. Hu, "A digital SIW-slot antenna array with FPGA implementation of beamforming," *Sci. Rep.*, vol.12, 8927, May 2022.
- [20] R.E. Collin, "Waveguides and cavities," *Field Theory of Guided Waves*, pp.329–410, IEEE, 1991.
- [21] E.H. Dinan and B. Jabbari, "Spreading codes for direct sequence CDMA and wideband CDMA cellular networks," *IEEE Commun. Mag.*, vol.36, no.9, pp.48–54, Sept. 1998.
- [22] Skyworks, "Design with PIN diodes," Skyworks Solutions, Inc., https://www.skyworksinc.com/-/media/skyworks/documents/products/1-100/Design_With_PIN_Diodes_200312E.pdf, July 2023.
- [23] Skyworks, "SMP1345 series: very low capacitance, plastic packaged silicon PIN diodes," Skyworks Solutions, Inc., https://www.skyworksinc.com/-/media/skyworks/documents/products/101-200/smp1345_series_200046u.pdf, July 2023.
- [24] Y. Miura, J. Hirokawa, M. Ando, Y. Shibuya, and G. Yoshida, "Double-layer full-corporate-feed hollow-waveguide slot array antenna in the 60-GHz band," *IEEE Trans. Antennas Propag.*, vol.59, no.8, pp.2844–2851, Aug. 2011.
- [25] R. Schmidt, "Multiple emitter location and signal parameter estimation," *IEEE Trans. Antennas Propag.*, vol.34, no.3, pp.276–280, March 1986.
- [26] W.K. Pratt, J. Kane, and H.C. Andrews, "Hadamard transform image coding," *Proc. IEEE*, vol.57, no.1, pp.58–68, Jan. 1969.
- [27] M.P. Deisenroth, A.A. Faisal, and C. S Ong, *Mathematics for Machine Learning*, Cambridge University Press, Cambridge, 2020.
- [28] G.B. Arfken and H.J. Weber, *Mathematical Methods for Physicists*, 5th ed., Academic Press, San Diego, 2000.

Appendix A: Walsh Hadamard Code

The Walsh Hadamard (WH) codes are based on the Hadamard matrices, which are square arrays of +1 and -1 and whose rows or columns are completely orthogonal to each other. The Hadamard matrices are generated as follows [26]:

$$\mathbf{H}_2 = \begin{bmatrix} 1 & 1 \\ 1 & -1 \end{bmatrix}, \quad \mathbf{H}_{2N} = \begin{bmatrix} \mathbf{H}_N & \mathbf{H}_N \\ \mathbf{H}_N & -\mathbf{H}_N \end{bmatrix} \quad (\text{A-1})$$

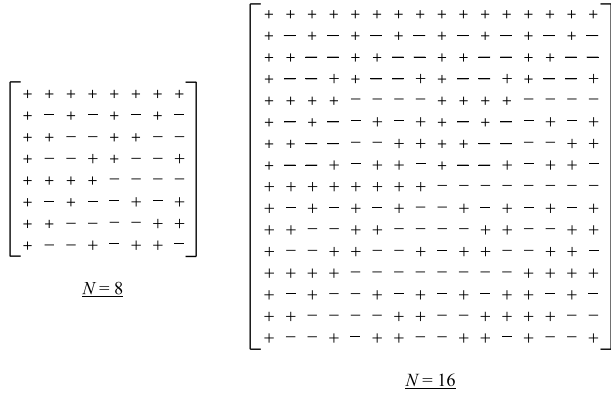


Fig. A.1 The Hadamard matrices of orders 8 and 16. + and - indicate +1 and -1, respectively.

where the subscripts indicate the orders of the Hadamard matrices. We show the Hadamard matrices of orders 8 and 16 in Fig. A.1 (the signs of ± 1 are only shown). The WH code corresponds to one of the row(column) vectors of the Hadamard matrices. The orthogonality of the WH codes can also be expressed as follows:

$$\frac{1}{N} \mathbf{h}_p \mathbf{h}_q^T = \begin{cases} 1 & \text{for } p = q \\ 0 & \text{for } p \neq q \end{cases} \quad (\text{A.2})$$

where \mathbf{h}_p and \mathbf{h}_q are the p th and q th row vectors of the Hadamard matrix of order N , respectively.

We now consider a vector Δ_q obtained by replacing +1 of \mathbf{h}_q by $(1 + \delta_q^{(+)})$ and -1 by $-(1 + \delta_q^{(-)})$. Using a property of an orthogonal matrix [27], the Euclidean norm of $\mathbf{H}_N \Delta_q^T$ can be expressed as follows:

$$\frac{1}{N} \|\mathbf{H}_N \Delta_q^T\|^2 = \|\Delta_q^T\|^2. \quad (\text{A.3})$$

When $q \neq 1$, the right side of (A.3) is $N\{(1 + \delta_q^{(+)})^2 + (1 + \delta_q^{(-)})^2\}/2$. The first and q th elements of $\mathbf{H}_N \Delta_q^T$ are $N(\delta_q^{(+)} - \delta_q^{(-)})/2$ and $N(2 + \delta_q^{(+)} + \delta_q^{(-)})/2$, respectively, and a sum of squares of them becomes $N^2\{(1 + \delta_q^{(+)})^2 + (1 + \delta_q^{(-)})^2\}/2$. To satisfy (A.3), therefore, the other elements of $\mathbf{H}_N \Delta_q^T$ must be all 0. Similarly, when $q = 1$, the right side of (A.4) is $N(1 + \delta_q^{(+)})^2$, and the first element of $\mathbf{H}_N \Delta_q^T$ is $N(1 + \delta_q^{(+)})$. Therefore, the other elements of $\mathbf{H}_N \Delta_q^T$ must be all 0. Since each element of $\mathbf{H}_N \Delta_q^T$ is a dot product of \mathbf{h}_p and Δ_q^T , the following orthogonality is then obtained:

$$\mathbf{h}_p \Delta_q^T = 0 \quad \text{for } p \neq q, p \neq 1. \quad (\text{A.4})$$

Appendix B: SNR Calculation

The average power of the interference signal for the m th slot pair is given by

$$E[|S_{m,i}(t)|^2] = E \left[\left| \frac{g}{T_b} \int_0^{T_b} n(t) c_m(t) dt \right|^2 \right]. \quad (\text{A.5})$$

Using the Schwarz's inequality [28], the right side of (A.5) becomes

$$\begin{aligned} & E \left[\left| \frac{g}{T_b} \int_0^{T_b} n(t) c_m(t) dt \right|^2 \right] \\ & \leq \frac{|g|^2}{T_b^2} E \left[\int_0^{T_b} |n(t)|^2 dt \cdot \int_0^{T_b} |c_m(t)|^2 dt \right] \\ & = \frac{|g|^2}{T_b} \int_0^{T_b} E[|n(t)|^2] dt = |g|^2 \sigma_n^2. \end{aligned} \quad (\text{A.6})$$

Therefore, the worst-case SNR at the element output becomes (12).

Next, we consider an SNR at the array output. When we assume that all incident signals to the slot pairs have an equal power, the gains of each slot pair are identical ($|f_{m\phi}|^2 = G_e$), and the amplitude of transmission characteristics of each slot pair through the waveguide are identical ($|\alpha_m| = \alpha_0$), the maximum average power of the combined desired signal is then calculated as

$$\begin{aligned} E \left[\left| \sum_{m=1}^M w_m S_{m,d}(t) \right|^2 \right] & = E \left[\left| g \sum_{m=1}^M w_m \alpha_m f_{m\phi} S_m(t) \right|^2 \right] \\ & = M^2 |g|^2 \alpha_0^2 G_e P_s. \end{aligned} \quad (\text{A.7})$$

where w_m are excitation weights and have a unity amplitude. Similarly, a combined interference signal at the array output is given by

$$\begin{aligned} \sum_{m=1}^M w_m S_{m,i}(t) & = \frac{g}{T_b} \sum_{m=1}^M w_m \int_0^{T_b} n(t) c_m(t) dt \\ & = \frac{g}{T_b} \int_0^{T_b} n(t) \sum_{m=1}^M w_m c_m(t) dt. \end{aligned} \quad (\text{A.8})$$

Using the Schwarz's inequality and the orthogonality of the WH codes, an average power of the combined interference signal is then calculated as

$$\begin{aligned} & E \left[\left| \frac{g}{T_b} \int_0^{T_b} n(t) \sum_{m=1}^M w_m c_m(t) dt \right|^2 \right] \\ & \leq \frac{|g|^2}{T_b^2} \int_0^{T_b} E[|n(t)|^2] dt \cdot E \left[\int_0^{T_b} \left| \sum_{m=1}^M w_m c_m(t) \right|^2 dt \right] \\ & = \frac{|g|^2 \sigma_n^2}{T_b} E \left[\int_0^{T_b} \sum_{m=1}^M |w_m|^2 c_m^2(t) dt \right] \\ & = \frac{|g|^2 \sigma_n^2}{T_b} \cdot M T_b = M |g|^2 \sigma_n^2. \end{aligned} \quad (\text{A.9})$$

Using (A.8) and (A.9), the SNR at the array output becomes (13).



Narihiro Nakamoto received the B.E. and M.E. degrees in electrical engineering from Kyoto University, Kyoto, Japan, in 2005 and 2007, respectively. In 2007, he joined Mitsubishi Electric Corporation, Kanagawa, Japan. From 2010 to 2012, he was with Advanced Telecommunications Research Institute International (ATR) Wave Engineering Laboratories, Kyoto, Japan. In 2012, he returned to Mitsubishi Electric Corporation and has been engaged in research and development on array antennas for

satellite communication and radar systems. He received the IEEE Antennas and Propagation Society Tokyo Chapter Young Engineer Award in 2013 and the Young Engineer Award of IEICE in 2012. He is a member of IEEE.



Naoki Shinohara received the B.E. degree in electronic engineering, the M.E. and Ph.D (Eng.) degrees in electrical engineering from Kyoto University, Japan, in 1991, 1993 and 1996, respectively. He was a research associate in Kyoto University from 1996. From 2010, he has been a professor in Kyoto University. He has been engaged in research on Solar Power Station/Satellite and Microwave Power Transmission system. He was IEEE MTT-S Distinguished Microwave Lecturer (2016–18), and is

IEEE AdCom member, IEEE MTT-S Technical Committee 25 (Wireless Power Transfer and Conversion) former chair and member, IEEE MTT-S MGA (Member Geographic Activities) Region 10 regional coordinator, IEEE WPT Initiative Member, IEEE MTT-S Kansai Chapter TPC member, IEEE Wireless Power Transfer Conference founder and Steering committee member, URSI commission D chair, international journal of Wireless Power Transfer (Hindawi) executive editor, the first chair and technical committee member on IEICE Wireless Power Transfer, Japan Society of Electromagnetic Wave Energy Applications adviser, Space Solar Power Systems Society vice chair, Wireless Power Transfer Consortium for Practical Applications (WiPoT) chair, and Wireless Power Management Consortium (WPMc) chair. His books are “Wireless Power Transfer via Radiowaves” (ISTE Ltd. and John Wiley & Sons, Inc.), “Recent Wireless Power Transfer Technologies Via Radio Waves (ed.)” (River Publishers), and “Wireless Power Transfer: Theory, Technology, and Applications (ed.)” (IET), and some Japanese textbooks of WPT.



Kazunari Kihira received the B.S., M.S., and Ph.D. degrees in electrical and computer engineering from the Nagoya Institute of Technology, Japan, in 1996, 1998, and 2007, respectively. In 1998, he joined Mitsubishi Electric Corporation, Kanagawa, Japan. His current research interests include phased array and adaptive antenna. He was a recipient of the Young Engineer Award of the IEICE in 2001 and the IEEE Antennas and Propagation Society Japan Chapter Young Engineer Award in 2005. He is a

member of the IEEE.



Toru Fukasawa was born in Tokyo, Japan, in 1969. He received the B.E., M.E., and Ph.D. degrees in electronic engineering from Hokkaido University, Sapporo, Japan, in 1992, 1994, and 2004, respectively. In 1994, he joined the Mitsubishi Electric Corporation, Tokyo, Japan. His current research interests include small antenna analysis and measurement methods. He received the Young Engineer Award in 2000 and the Best Paper Award in 2011, 2012, 2016, and 2018 from IEICE. He is a member of IEEE.



Yoshio Inasawa received B.E., M.E., and Ph.D. degrees in Electrical and Electronics Engineering from the Tokyo Institute of Technology in 1991, 1993, and 2008, respectively. In 1993, he joined Mitsubishi Electric Corporation, Tokyo. Since then, he has been engaged in research on electromagnetic field analysis and reflector antennas. He is currently a manager in the Antenna Technology Department of the Information Technology Research and Development Center, Mitsubishi Electric Corporation. Dr. Inasawa received the Young Researcher's Award of IEICE Japan in 1998 and the R&D 100 Awards in 2005. He is a senior member of the IEEE.

received the Young Researcher's Award of IEICE Japan in 1998 and the R&D 100 Awards in 2005. He is a senior member of the IEEE.